

Universal quantum gates on electron-spin qubits with quantum dots inside single-side optical microcavities*

Hai-Rui Wei¹ and Fu-Guo Deng^{1,2,†}

¹*Department of Physics, Applied Optics Beijing Area Major Laboratory,
Beijing Normal University, Beijing 100875, China*

²*State key Laboratory of Networking and Switching Technology,
Beijing University of Posts and Telecommunications, Beijing 100876, China*

We present some compact quantum circuits for a deterministic quantum computing on electron-spin qubits assisted by quantum dots inside single-side optical microcavities, including the CNOT, Toffoli, and Fredkin gates. They are constructed by exploiting the giant optical Faraday rotation induced by a single-electron spin in a quantum dot inside a single-side optical microcavity as a result of cavity quantum electrodynamics. Our universal quantum gates have some advantages. First, all the gates are accomplished with a success probability of 100% in principle. Second, our schemes require no additional electron-spin qubits and they are achieved by some input-output processes of a single photon. Third, our circuits for these gates are simple and economic. Moreover, our devices for these gates work in both the weak coupling and the strong coupling regimes, and they are feasible in experiment.

PACS numbers: 03.67.Lx, 42.50.Ex, 42.50.Pq, 78.67.Hc

I. INTRODUCTION

In quantum computing, a quantum algorithm is usually realized by a sequence of quantum gates [1]. Constructing compact quantum gates is crucial for building a quantum computer. It has been proven that any quantum entangling gate supplementing with single-qubit gates can implement a universal quantum computing [2]. The controlled-not (CNOT) gate is a universal two-qubit gate and it attracts much attention. As for multi-qubit quantum systems, attention was mainly focused on the three-qubit Toffoli and Fredkin gates as they can be used to implement any multi-qubit quantum computing with Hadamard gates [3, 4].

Up to now, many important proposals have been proposed for physically implementing quantum gates [5–7]. For example, in 2001, Knill *et al.* [8] proposed a probabilistic scheme for implementing a CNOT gate on two photonic qubits by using linear optical elements, additional photons, and postselection. Based on cross-Kerr nonlinearity or charge detection, Nemoto *et al.* [9], Lin *et al.* [10], and Beenakker *et al.* [11] provided some interesting proposals for a deterministic quantum computing. In these schemes, some additional qubits are employed. A strong cross-Kerr nonlinearity is still a big challenge in experiment at present. To achieve a nontrivial nonlinearity between two individual qubits for a deterministic quantum computation with the present experimental techniques, an appealing platform for quantum information processing with an artificial atom and a cavity is proposed [12, 13].

A quantum system combining a cavity and an artificial atom, such as a quantum dot (QD), a superconducting qubit, or a diamond nitrogen-vacancy center, is a perfect platform for quantum information processing because of its long coherence time and its good scalability. By utilizing such a platform, some interesting schemes were proposed for implementing the quantum gates on hybrid photon-matter systems [12–15]. Based on the QD-cavity platform, a scalable deterministic quantum computation on photonic qubits [16–18] and a deterministic photonic spatial-polarization hyper-CNOT gate [19] were proposed recently. The quantum circuits for the universal gates on superconducting qubits [20, 21] or diamond nitrogen-vacancy center qubits [22–24] assisted by optical microcavities were designed as well. Constructing universal quantum gates compactly can reduce the quantum resource needed and their errors.

A QD system is one of the promising candidates for quantum information processing and quantum state storage in solid-state quantum systems. The coherence time of a QD can be extended to μs by using spin echo techniques [25–27]. The single QD spin manipulation which is crucial for the implementation of single-qubit gates, can be achieved by using pulsed magnetic resonance techniques, nanosecond microwave pulses, or picosecond/femtosecond optical pulses [28–30]. Due to the external magnetic field and the short dephasing time, the magnetic resonance techniques are not compatible with our work. In our work, the 90° rotation on the electron-spin qubit around the optical axis can be

* Published in Opt. Express **22**, 593-607 (2014)

† Corresponding author: fgdeng@bnu.edu.cn

achieved by using a single photon, and the 180° rotation can be achieved by using a single photon which interacts with the QD twice [31].

In this paper, we present some compact quantum circuits for a universal quantum computing on an electron-spin system assisted by the QDs inside single-side optical microcavities. Based on the giant circular birefringence induced by a QD-cavity system as a result of cavity quantum electrodynamics [12, 13], we construct the CNOT, Toffoli, and Fredkin gates on a stationary electron-spin system, achieved by some input-output processes of a single photon. Our schemes are simple and economic. They are accomplished with a success probability of 100% in principle and they do not require the additional electron-spin qubits which are employed in [9–11]. Our circuits for implementing the CNOT and Toffoli gates are especially compact. The electron qubits involved in these gates are stationary, which reduces the interaction between the spins and their environments, different from [11]. Moreover, our quantum circuits for the Toffoli and Fredkin gates beat their synthesis with two-qubit entangling gates and single-qubit gates largely. With current technology, these universal solid-state quantum gates are feasible.

II. COMPACT QUANTUM CIRCUIT FOR A CNOT GATE ON A STATIONARY ELECTRON-SPIN SYSTEM

A. A singly charged quantum dot in a single-side optical resonant microcavity

Figure 1 depicts the single-side QD-cavity system used in our schemes, i.e., a self-assembled In(Ga)As QD or a GaAs interface QD embedded in an optical resonant microcavity with one mirror partially reflective and the another one 100% reflective [12, 13]. According to Pauli's exclusion principle, a negatively charged exciton (X^-) consisting of two electrons bound to one hole can be optically excited when an excess electron is injected into the QD [19]. In Fig. 1, $|\uparrow\rangle$ and $|\downarrow\rangle$ represent the spins of the excess electron with the angular momentum projections $J_z = +1/2$ and $J_z = -1/2$ along the cavity axis, respectively. $|\uparrow\rangle$ and $|\downarrow\rangle$ represent the hole-spin states with $J_z = +3/2$ and $J_z = -3/2$, respectively. $|R\rangle$ and $|L\rangle$ present the right-circularly polarized photon and the left-circularly polarized photon, respectively. In 2008, Hu *et al.* [12, 13] showed that the L-polarized photon ($|L\rangle$) drives $|\uparrow\rangle$ transform into $|\uparrow\downarrow\rangle$ and the R-polarized photon ($|R\rangle$) drives $|\downarrow\rangle$ transform into $|\downarrow\uparrow\rangle$, respectively, due to Pauli's exclusion principle. The coupled R-polarized (L-polarized) photon and the uncoupled L-polarized (R-polarized) photon acquire different phases and amplitudes when they are reflected by the cavity. The reflection coefficient

$$r(\omega) = |r(\omega)|e^{i\varphi(\omega)} = 1 - \frac{\kappa[i(\omega_{X^-} - \omega) + \frac{\gamma}{2}]}{[i(\omega_{X^-} - \omega) + \frac{\gamma}{2}][i(\omega_c - \omega) + \frac{\kappa}{2} + \frac{\kappa_s}{2}] + g^2} \quad (1)$$

can be obtain by solving the Heisenberg equations of the motion for the cavity mode \hat{a} and the dipole operation σ_- driven by the input field \hat{a}_{in} , and combing the relation between the input field \hat{a}_{in} and the output field \hat{a}_{out} in the weak excitation approximation [32]

$$\begin{aligned} \frac{d\hat{a}}{dt} &= -\left[i(\omega_c - \omega) + \frac{\kappa}{2} + \frac{\kappa_s}{2}\right]\hat{a} - g\sigma_- - \sqrt{\kappa}\hat{a}_{in} + \hat{H}, \\ \frac{d\sigma_-}{dt} &= -\left[i(\omega_{X^-} - \omega) + \frac{\gamma}{2}\right]\sigma_- - g\sigma_z\hat{a} + \hat{G}, \\ \hat{a}_{out} &= \hat{a}_{in} + \sqrt{\kappa}\hat{a}. \end{aligned} \quad (2)$$

Here ω_c and ω are the frequencies of the cavity mode and the input single photon, respectively. ω_{X^-} is the frequency of the dipole transition of the negatively charged exciton X^- . g is the coupling strength between the cavity mode and X^- . $\kappa/2$ and $\kappa_s/2$ are the decay rate and the side leakage rate of the cavity field, respectively. $\gamma/2$ represents the decay rate of X^- . \hat{H} and \hat{G} are the noise operators related to the reservoirs.

Hu *et al.* [12, 13] showed that $|r_0(\omega)| \simeq 1$ for all ω if $\kappa_s \ll \kappa$. If $\kappa_s \ll \kappa$ and $g > (\kappa, \gamma)$, one can see that $|r_h(\omega)| \simeq 1$ when $|\omega - \omega_c| \ll g$. Here $r_0(\omega)$ and $r_h(\omega)$ are given by Eq. (1) with $g = 0$ and $g \neq 0$, respectively. When κ_s is negligible, the transformations induced by the interaction between the QD and the input single photon can be expressed as follows:

$$\begin{aligned} (|R\rangle + |L\rangle)|\uparrow\rangle &\xrightarrow{\text{cav}} (e^{i\varphi_0}|R\rangle + e^{i\varphi_h}|L\rangle)|\uparrow\rangle = e^{i\varphi_0}(|R\rangle + e^{i(\varphi_h - \varphi_0)}|L\rangle)|\uparrow\rangle, \\ (|R\rangle + |L\rangle)|\downarrow\rangle &\xrightarrow{\text{cav}} e^{i\varphi_h}|R\rangle|\downarrow\rangle + e^{i\varphi_0}|L\rangle|\downarrow\rangle = e^{i\varphi_0}(e^{i(\varphi_h - \varphi_0)}|R\rangle + |L\rangle)|\downarrow\rangle. \end{aligned} \quad (3)$$

Here $\varphi_0 = \arg[r_0(\omega)]$ and $\varphi_h = \arg[r_h(\omega)]$. We consider the case that the QD is resonant with the cavity mode and it interacts with the resonant single photon (i.e., $\omega_{X^-} = \omega_c = \omega$) in the conditions $\kappa_s \ll \kappa$ and $g > (\kappa, \gamma)$ below. In this

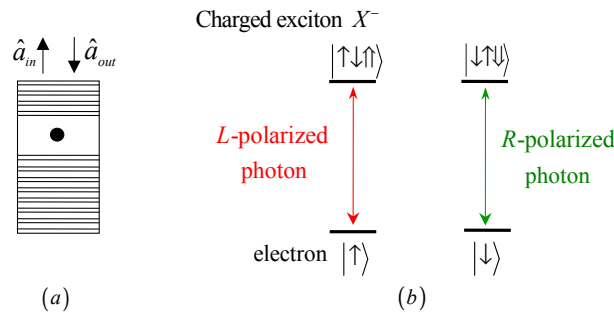


FIG. 1: (a) Schematic diagram of a coupled single-side QD-cavity system. (b) The energy-level structure of a QD-cavity system [12, 13]. $|\uparrow\rangle \rightarrow |\uparrow\downarrow\uparrow\rangle$ is driven by the left-circularly polarized photon ($|L\rangle$) and $|\downarrow\rangle \rightarrow |\downarrow\uparrow\downarrow\rangle$ is driven by the right-circularly polarized photon ($|R\rangle$), respectively.

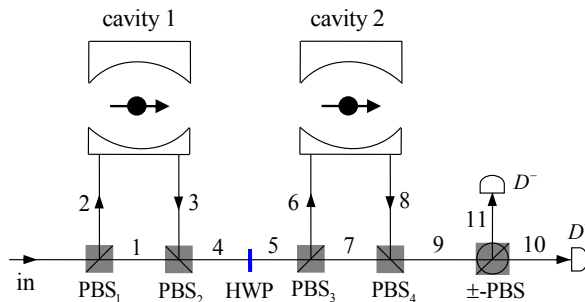


FIG. 2: Compact quantum circuit for deterministically implementing a CNOT gate on two QD electron-spin qubits with a single-photon medium. The polarizing beam splitter PBS_i ($i = 1, 2, 3, 4$) in the basis $\{|R\rangle, |L\rangle\}$ transmits the R -polarized photon and reflects the L -polarized photon. BS is a 50:50 beam splitter. The \pm -PBS transmits the photon in the state $|+\rangle = (|R\rangle + |L\rangle)/\sqrt{2}$ and reflects the photon in the state $|-\rangle = (|R\rangle - |L\rangle)/\sqrt{2}$. The half wave plate (HWP) set to 22.5° induces the transformations $|R\rangle \xrightarrow{H_p} (|R\rangle + |L\rangle)/\sqrt{2}$ and $|L\rangle \xrightarrow{H_p} (|R\rangle - |L\rangle)/\sqrt{2}$. D^+ and D^- represent two single-photon detectors.

case, $e^{i\varphi_0} = -1$ and $e^{i\varphi_h} = 1$. That is, $\varphi_h - \varphi_0 = \pm\pi$. The rules of the input states changing under the interaction of the photon and the cavity can be summarized as follows:

$$\begin{aligned} |R\rangle|\uparrow\rangle &\xrightarrow{\text{cav}} -|R\rangle|\uparrow\rangle, & |L\rangle|\uparrow\rangle &\xrightarrow{\text{cav}} |L\rangle|\uparrow\rangle, \\ |R\rangle|\downarrow\rangle &\xrightarrow{\text{cav}} |R\rangle|\downarrow\rangle, & |L\rangle|\downarrow\rangle &\xrightarrow{\text{cav}} -|L\rangle|\downarrow\rangle. \end{aligned} \quad (4)$$

In 2011, Young *et al.* [33] measured the macroscopic phase shift of the reflected photon from a single-side pillar microcavity induced by a single QD in experiment. In a realistic cavity system, although it is hard to achieve the phase shift $\varphi_h - \varphi_0 = \pm\pi$ due to the side leakage and the cavity loss [34], the phase shift $\pm\pi/2$ can be actually achieved in a QD-single-side-cavity system and it has been demonstrated by Hu's group [31]. When $\kappa_s < 1.3\kappa$, the phase shift $\pm\pi/2$ can be achieved; otherwise, it cannot be achieved. The phase shift π in our schemes can be achieved by a single photon which interacts with the QD twice. The above model works for a general polarization-degenerate cavity mode, including the micropillar [35–37], H1 photonic crystal [38, 39], and fiber-based [40] cavities.

Utilizing the optical circular birefringence induced by cavity quantum electrodynamics, the QD-cavity platform has been used to generate the maximally entangled states [12, 13, 31, 41–43], construct the conditional phase gate on hybrid photon-QD systems [12, 13], and design the hyper-CNOT gate on photonic qubits [19]. Based on the double-side one [41], some universal quantum gates on photonic qubits [16, 17] and hybrid photon-QD systems [15] have been proposed. In 2011, Wang *et al.* [44] proposed a scheme for implementing a quantum repeater, resorting to the QDs in double-side cavities. In the following, we discuss the implementation of a deterministic quantum computing with QD-single-side-cavity systems, shown in Fig. 1. The QD-double-side-cavity system is robust to the transmission and the reflection coefficients, while the side leakage rate of the QD-single-side-cavity system is lower than the double-side one.

B. Compact circuit for a CNOT gate on a stationary electron-spin system

The principle for implementing a CNOT gate on the two stationary electron-spin qubits in the QDs confined in single-side resonant optical microcavities is shown in Fig. 2. It flips the state of the target qubit when the control qubit is in the state $|\downarrow\rangle$. Suppose the input state of the quantum system composed of the control and the target qubits (confined in the cavities 1 and 2, respectively) are initially prepared as

$$|\psi\rangle_{\text{in}}^e = |\uparrow\rangle_c(\alpha_1|\uparrow\rangle_t + \alpha_2|\downarrow\rangle_t) + |\downarrow\rangle_c(\alpha_3|\uparrow\rangle_t + \alpha_4|\downarrow\rangle_t). \quad (5)$$

Here $\sum_{i=1}^4 |\alpha_i|^2 = 1$. The input single photon is prepared in the equal polarization superposition state $|\psi\rangle^p = \frac{1}{\sqrt{2}}(|R\rangle + |L\rangle)$.

Let us introduce the principle of our deterministic CNOT gate on two stationary electron-spin qubits. As depicted in Fig. 2, a single photon is injected into the input port *in*, and its *R*-polarized component is transmitted to the spatial model 1 by the polarizing beam splitter PBS_1 and then arrives at PBS_2 directly, while its *L*-polarized component is reflected to the spatial model 2 for interacting with the QD inside the cavity 1. After the photon emitting from the spatial models 1 and 3 arrives at PBS_2 simultaneously, a Hadamard operation H_p is performed on it. That is, we let the photon pass through the half-wave plate (HWP) oriented at 22.5° , which results in the transformations as follows:

$$|R\rangle \xrightarrow{H_p} \frac{1}{\sqrt{2}}(|R\rangle + |L\rangle), \quad |L\rangle \xrightarrow{H_p} \frac{1}{\sqrt{2}}(|R\rangle - |L\rangle). \quad (6)$$

Before and after the photon passes through the block composed of PBS_3 , the QD inside the cavity 2, and PBS_4 , a Hadamard operation H_e is performed on the electron spin in the QD inside the cavity 2, respectively. Here H_e completes the transformations as follows:

$$|\uparrow\rangle \xrightarrow{H_e} \frac{1}{\sqrt{2}}(|\uparrow\rangle + |\downarrow\rangle), \quad |\downarrow\rangle \xrightarrow{H_e} \frac{1}{\sqrt{2}}(|\uparrow\rangle - |\downarrow\rangle). \quad (7)$$

The evolution of the whole system composed of a single-photon medium and the QDs inside the cavities 1 and 2 induced by the above operations ($\text{PBS}_1 \rightarrow \text{cavity 1} \rightarrow \text{PBS}_2 \rightarrow \text{HWP} \rightarrow H_{e_2} \rightarrow \text{PBS}_3 \rightarrow \text{cavity 2} \rightarrow \text{PBS}_4 \rightarrow H_{e_2}$) can be described as follows:

$$|\psi\rangle^p \otimes |\psi\rangle_{\text{in}}^e \rightarrow |R\rangle_9 |\uparrow\rangle_c(\alpha_1|\uparrow\rangle_t + \alpha_2|\downarrow\rangle_t) + |L\rangle_9 |\downarrow\rangle_c(\alpha_3|\downarrow\rangle_t + \alpha_4|\uparrow\rangle_t). \quad (8)$$

Here and below, we use $|R\rangle_i$ ($|L\rangle_i$) to denote the photon in the state $|R\rangle$ ($|L\rangle$) emitting from the spatial mode i and use H_{e_i} to denote a Hadamard operation performed on the i -th QD-spin qubit.

Next, the single photon is measured in the basis $\{|\pm\rangle = (|R\rangle \pm |L\rangle)/\sqrt{2}\}$ by the detectors D^+ and D^- . From Eq. (8), one can see that the response of the detector D^+ indicates that the CNOT gate on the two electron-spin qubits succeeds; if the detector D^- is clicked, after we perform a classical feed-forward operation $\sigma_z = |\uparrow\rangle\langle\uparrow| - |\downarrow\rangle\langle\downarrow|$ on the control qubit, the CNOT gate is accomplished as well. That is, the output state of the system composed of the control and the target qubits confined in the cavities 1 and 2 becomes

$$|\psi\rangle_{\text{in}}^e \xrightarrow{\text{CNOT}} |\psi\rangle_{\text{out}}^e = \alpha_1|\uparrow\rangle_c|\uparrow\rangle_t + \alpha_2|\uparrow\rangle_c|\downarrow\rangle_t + \alpha_3|\downarrow\rangle_c|\downarrow\rangle_t + \alpha_4|\downarrow\rangle_c|\uparrow\rangle_t. \quad (9)$$

The quantum circuit shown in Fig. 2 can be used to implement a CNOT gate on the two-qubit electron-spin system in a deterministic way, which implements a not operation on the target qubit if and only if (iff) the control qubit is in the state $|\downarrow\rangle$.

III. COMPACT QUANTUM CIRCUIT FOR A TOFFOLI GATE ON THREE ELECTRON-SPIN QUBITS IN QDS

The principle for implementing a Toffoli gate on a three-qubit electron-spin system is shown in Fig. 3. It is used to flip the state of the target qubit iff both the two control qubits are in the state $|\downarrow\rangle$. Suppose the quantum system, which is composed of the three independent excess electrons inside the cavities 1, 2, and 3 that act as the first control qubit, the second control qubit, and the target qubit, respectively, is initially prepared in an arbitrary state

$$\begin{aligned} |\Xi\rangle_{\text{in}}^e = & |\uparrow\rangle_{c_1}|\uparrow\rangle_{c_2}(\alpha_1|\uparrow\rangle_t + \alpha_2|\downarrow\rangle_t) + |\uparrow\rangle_{c_1}|\downarrow\rangle_{c_2}(\alpha_3|\uparrow\rangle_t + \alpha_4|\downarrow\rangle_t) \\ & + |\downarrow\rangle_{c_1}|\uparrow\rangle_{c_2}(\alpha_5|\uparrow\rangle_t + \alpha_6|\downarrow\rangle_t) + |\downarrow\rangle_{c_1}|\downarrow\rangle_{c_2}(\alpha_7|\uparrow\rangle_t + \alpha_8|\downarrow\rangle_t). \end{aligned} \quad (10)$$

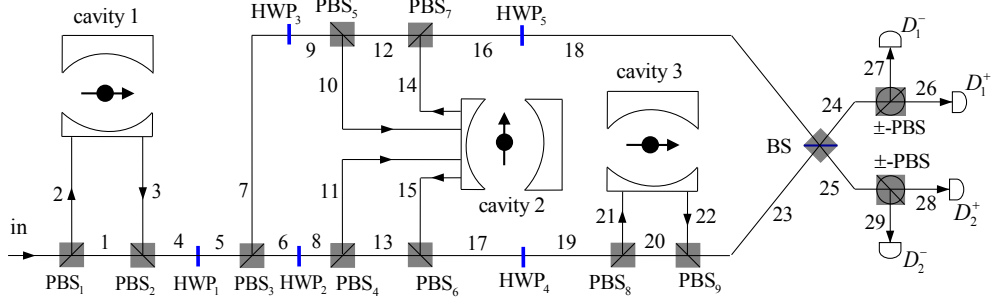


FIG. 3: Compact quantum circuit for deterministically implementing a Toffoli gate on three stationary electron-spin qubits in QDs with the input-output processes of a single-photon medium.

Here $\sum_{i=1}^8 |\alpha_i|^2 = 1$.

Next, we will specify the evolution of the system from the input state to the output state for characterizing the performance of our Toffoli gate. As illustrated in Fig. 3, our scheme for a Toffoli gate on a three-qubit electron-spin system can be achieved with four steps.

First, an input single photon in the state $|\Xi\rangle^p = \frac{1}{\sqrt{2}}(|R\rangle - |L\rangle)$ goes through the block composed of PBS_1 , the QD inside the cavity 1, and PBS_2 , and then an H_p is performed on it (i.e., let the photon go through HWP_1). Based on the argument as made in Sec. II B, one can see that the above operations ($\text{PBS}_1 \rightarrow \text{cavity 1} \rightarrow \text{PBS}_2 \rightarrow \text{HWP}_1$) transform the state of the complicated system composed of the single photon and the three QD-spin qubits from $|\Xi_0\rangle$ into $|\Xi_1\rangle$. Here

$$\begin{aligned} |\Xi_0\rangle &= |\Xi\rangle^p \otimes |\Xi\rangle_{\text{in}}^e, \\ |\Xi_1\rangle &= |L\rangle_5 |\uparrow\rangle_{c_1} |\uparrow\rangle_{c_2} (\alpha_1 |\uparrow\rangle_t + \alpha_2 |\downarrow\rangle_t) + |L\rangle_5 |\uparrow\rangle_{c_1} |\downarrow\rangle_{c_2} (\alpha_3 |\uparrow\rangle_t + \alpha_4 |\downarrow\rangle_t) \\ &\quad + |R\rangle_5 |\downarrow\rangle_{c_1} |\uparrow\rangle_{c_2} (\alpha_5 |\uparrow\rangle_t + \alpha_6 |\downarrow\rangle_t) + |R\rangle_5 |\downarrow\rangle_{c_1} |\downarrow\rangle_{c_2} (\alpha_7 |\uparrow\rangle_t + \alpha_8 |\downarrow\rangle_t). \end{aligned} \quad (11)$$

Second, PBS_3 transforms $|R\rangle_5$ and $|L\rangle_5$ into $|R\rangle_6$ and $|L\rangle_7$, respectively. Before and after the component $|R\rangle_6$ ($|L\rangle_7$) of the photon goes through the block composed of PBS_4 , the QD inside the cavity 2, and PBS_6 (PBS_5 , the QD inside the cavity 2, and PBS_7), an H_p is performed on it with HWP_2 and HWP_4 (HWP_3 and HWP_5). The operations ($\text{HWP}_2 \rightarrow \text{PBS}_4 \rightarrow \text{cavity 2} \rightarrow \text{PBS}_6 \rightarrow \text{HWP}_4$ and $\text{HWP}_3 \rightarrow \text{PBS}_5 \rightarrow \text{cavity 2} \rightarrow \text{PBS}_7 \rightarrow \text{HWP}_5$) transform the state of the complicated system into

$$\begin{aligned} \rightarrow |\Xi_2\rangle &= |L\rangle_{18} |\uparrow\rangle_{c_1} |\uparrow\rangle_{c_2} (\alpha_1 |\uparrow\rangle_t + \alpha_2 |\downarrow\rangle_t) + |R\rangle_{18} |\uparrow\rangle_{c_1} |\downarrow\rangle_{c_2} (\alpha_3 |\uparrow\rangle_t + \alpha_4 |\downarrow\rangle_t) \\ &\quad + |R\rangle_{19} |\downarrow\rangle_{c_1} |\uparrow\rangle_{c_2} (\alpha_5 |\uparrow\rangle_t + \alpha_6 |\downarrow\rangle_t) + |L\rangle_{19} |\downarrow\rangle_{c_1} |\downarrow\rangle_{c_2} (\alpha_7 |\uparrow\rangle_t + \alpha_8 |\downarrow\rangle_t). \end{aligned} \quad (12)$$

Third, before and after the photon goes through the block composed of PBS_8 , the QD inside the cavity 3, and PBS_9 when it emits from the spatial model 19, an H_e is performed on the electron spin in the QD inside the cavity 3, respectively. These operations ($H_{e_3} \rightarrow \text{PBS}_8 \rightarrow \text{cavity 3} \rightarrow \text{PBS}_9 \rightarrow H_{e_3}$) complete the transformation

$$\begin{aligned} \rightarrow |\Xi_3\rangle &= |L\rangle_{18} |\uparrow\rangle_{c_1} |\uparrow\rangle_{c_2} (\alpha_1 |\uparrow\rangle_t + \alpha_2 |\downarrow\rangle_t) + |R\rangle_{18} |\uparrow\rangle_{c_1} |\downarrow\rangle_{c_2} (\alpha_3 |\uparrow\rangle_t + \alpha_4 |\downarrow\rangle_t) \\ &\quad + |R\rangle_{23} |\downarrow\rangle_{c_1} |\uparrow\rangle_{c_2} (\alpha_5 |\uparrow\rangle_t + \alpha_6 |\downarrow\rangle_t) + |L\rangle_{23} |\downarrow\rangle_{c_1} |\downarrow\rangle_{c_2} (\alpha_7 |\downarrow\rangle_t + \alpha_8 |\uparrow\rangle_t). \end{aligned} \quad (13)$$

Subsequently, the wave packet emitting from the spatial model 23 arrives at the 50:50 beam splitter (BS) with the wave packet emitting from the spatial model 18 simultaneously.

Fourth, the balanced BS, which completes the transformations

$$\begin{aligned} |R\rangle_{18} &\xrightarrow{\text{BS}} \frac{1}{\sqrt{2}}(|R\rangle_{24} + |R\rangle_{25}), & |L\rangle_{18} &\xrightarrow{\text{BS}} \frac{1}{\sqrt{2}}(|L\rangle_{24} + |L\rangle_{25}), \\ |R\rangle_{23} &\xrightarrow{\text{BS}} \frac{1}{\sqrt{2}}(|R\rangle_{24} - |R\rangle_{25}), & |L\rangle_{23} &\xrightarrow{\text{BS}} \frac{1}{\sqrt{2}}(|L\rangle_{24} - |L\rangle_{25}), \end{aligned} \quad (14)$$

transforms $|\Xi_3\rangle$ into the state

$$\begin{aligned}
\overset{\text{BS}}{\rightarrow} |\Xi_4\rangle = & \frac{|+\rangle_{26}}{2} \left[|\uparrow\rangle_{c_1} |\uparrow\rangle_{c_2} (\alpha_1 |\uparrow\rangle_t + \alpha_2 |\downarrow\rangle_t) + |\uparrow\rangle_{c_1} |\downarrow\rangle_{c_2} (\alpha_3 |\uparrow\rangle_t + \alpha_4 |\downarrow\rangle_t) \right. \\
& \left. + |\downarrow\rangle_{c_1} |\uparrow\rangle_{c_2} (\alpha_5 |\uparrow\rangle_t + \alpha_6 |\downarrow\rangle_t) + |\downarrow\rangle_{c_1} |\downarrow\rangle_{c_2} (\alpha_7 |\downarrow\rangle_t + \alpha_8 |\uparrow\rangle_t) \right] \\
& + \frac{|-\rangle_{27}}{2} \left[-|\uparrow\rangle_{c_1} |\uparrow\rangle_{c_2} (\alpha_1 |\uparrow\rangle_t + \alpha_2 |\downarrow\rangle_t) + |\uparrow\rangle_{c_1} |\downarrow\rangle_{c_2} (\alpha_3 |\uparrow\rangle_t + \alpha_4 |\downarrow\rangle_t) \right. \\
& \left. + |\downarrow\rangle_{c_1} |\uparrow\rangle_{c_2} (\alpha_5 |\uparrow\rangle_t + \alpha_6 |\downarrow\rangle_t) - |\downarrow\rangle_{c_1} |\downarrow\rangle_{c_2} (\alpha_7 |\downarrow\rangle_t + \alpha_8 |\uparrow\rangle_t) \right] \\
& + \frac{|+\rangle_{28}}{2} \left[|\uparrow\rangle_{c_1} |\uparrow\rangle_{c_2} (\alpha_1 |\uparrow\rangle_t + \alpha_2 |\downarrow\rangle_t) + |\uparrow\rangle_{c_1} |\downarrow\rangle_{c_2} (\alpha_3 |\uparrow\rangle_t + \alpha_4 |\downarrow\rangle_t) \right. \\
& \left. - |\downarrow\rangle_{c_1} |\uparrow\rangle_{c_2} (\alpha_5 |\uparrow\rangle_t + \alpha_6 |\downarrow\rangle_t) - |\downarrow\rangle_{c_1} |\downarrow\rangle_{c_2} (\alpha_7 |\downarrow\rangle_t + \alpha_8 |\uparrow\rangle_t) \right] \\
& + \frac{|-\rangle_{29}}{2} \left[-|\uparrow\rangle_{c_1} |\uparrow\rangle_{c_2} (\alpha_1 |\uparrow\rangle_t + \alpha_2 |\downarrow\rangle_t) + |\uparrow\rangle_{c_1} |\downarrow\rangle_{c_2} (\alpha_3 |\uparrow\rangle_t + \alpha_4 |\downarrow\rangle_t) \right. \\
& \left. - |\downarrow\rangle_{c_1} |\uparrow\rangle_{c_2} (\alpha_5 |\uparrow\rangle_t + \alpha_6 |\downarrow\rangle_t) + |\downarrow\rangle_{c_1} |\downarrow\rangle_{c_2} (\alpha_7 |\downarrow\rangle_t + \alpha_8 |\uparrow\rangle_t) \right]. \tag{15}
\end{aligned}$$

According to the outcomes of the measurement on the single photon in the basis $\{|\pm\rangle\}$, we perform the appropriate single-qubit operations on the qubits shown in Table I, and then the state of the solid-state quantum system composed of the three electron-spin qubits becomes

$$\begin{aligned}
|\Xi\rangle_{\text{out}}^e = & |\uparrow\rangle_{c_1} |\uparrow\rangle_{c_2} (\alpha_1 |\uparrow\rangle_t + \alpha_2 |\downarrow\rangle_t) + |\uparrow\rangle_{c_1} |\downarrow\rangle_{c_2} (\alpha_3 |\uparrow\rangle_t + \alpha_4 |\downarrow\rangle_t) \\
& + |\downarrow\rangle_{c_1} |\uparrow\rangle_{c_2} (\alpha_5 |\uparrow\rangle_t + \alpha_6 |\downarrow\rangle_t) + |\downarrow\rangle_{c_1} |\downarrow\rangle_{c_2} (\alpha_7 |\downarrow\rangle_t + \alpha_8 |\uparrow\rangle_t). \tag{16}
\end{aligned}$$

From Eqs. (11) and (16), one can see that the evolution $|\Xi\rangle_{\text{in}}^e \xrightarrow{\text{Toffoli}} |\Xi\rangle_{\text{out}}^e$ is accomplished. That is, the quantum circuit shown in Fig. 3 implements a Toffoli gate on the three stationary electron-spin qubits in QDs, and it flips the state of the target qubit inside the cavity 3 iff both the two control qubits inside the cavities 1 and 2, respectively, are in the state $|\downarrow\rangle$ with a successful probability of 100% in principle.

TABLE I: The relations between the measurement outcomes of the single photon and the classical feed-forward operations for implementing the Toffoli gate on the three stationary electron-spin qubits. $\sigma_z = |\uparrow\rangle\langle\uparrow| - |\downarrow\rangle\langle\downarrow|$. $I_2 = |\uparrow\rangle\langle\uparrow| + |\downarrow\rangle\langle\downarrow|$ is a 2×2 unit operation which means doing nothing on a qubit.

photon	Feed-forward		
	qubit c_1	qubit c_2	qubit t
$D_1^+ (+\rangle_{26})$	I_2	I_2	I_2
$D_1^- (-\rangle_{27})$	$-\sigma_z$	σ_z	I_2
$D_2^+ (+\rangle_{28})$	σ_z	I_2	I_2
$D_2^- (-\rangle_{29})$	I_2	$-\sigma_z$	I_2

IV. COMPACT QUANTUM CIRCUIT FOR A FREDKIN GATE ON A THREE-QUBIT ELECTRON-SPIN SYSTEM

Figure 4 depicts the principle of our scheme for implementing a Fredkin gate on a three-qubit electron-spin system assisted by the QDs inside single-side optical microcavities, which swaps the states of the two target qubits iff the control qubit is in the state $|\downarrow\rangle$. Suppose the input state of the system composed of the control qubit, the first target qubit, and the second target qubit inside the cavities 1, 2, and 3, respectively, is initially prepared as

$$\begin{aligned}
|\Pi\rangle_{\text{in}}^e = & |\uparrow\rangle_c |\uparrow\rangle_{t_1} (\alpha_1 |\uparrow\rangle_{t_2} + \alpha_2 |\downarrow\rangle_{t_2}) + |\uparrow\rangle_c |\downarrow\rangle_{t_1} (\alpha_3 |\uparrow\rangle_{t_2} + \alpha_4 |\downarrow\rangle_{t_2}) \\
& + |\downarrow\rangle_c |\uparrow\rangle_{t_1} (\alpha_5 |\uparrow\rangle_{t_2} + \alpha_6 |\downarrow\rangle_{t_2}) + |\downarrow\rangle_c |\downarrow\rangle_{t_1} (\alpha_7 |\uparrow\rangle_{t_2} + \alpha_8 |\downarrow\rangle_{t_2}). \tag{17}
\end{aligned}$$

Here $\sum_{i=1}^8 |\alpha_i|^2 = 1$. The input single photon is prepared in the state $|\Pi\rangle^p = \frac{1}{\sqrt{2}}(|R\rangle - |L\rangle)$.

Let us now describe the principle of our scheme for implementing a Fredkin gate on the three stationary electron-spin qubits in QDs in detail.

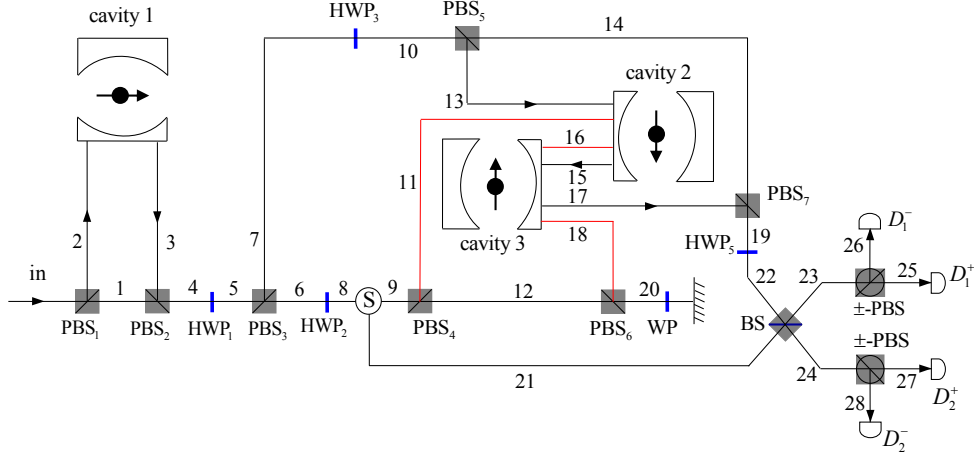


FIG. 4: Compact quantum circuit for determinately implementing a Fredkin gate on three QD-spin qubits with the input-output processes of a single-photon medium. Wave plate WP performs a Hadamard operation on the photon who goes through it two times in succession.

First, based on the argument as made in Sec. III, after the input photon goes through the block composed of PBS₁, the QD inside the cavity 1, and PBS₂, an H_p (i.e., let it go through HWP₁) is performed on it, and then the state of the whole system composed of the single photon and the three electron-spin qubits in the QDs confined in the cavities 1, 2, and 3 is transformed from $|\Pi_0\rangle$ into $|\Pi_1\rangle$ by the above operations (PBS₁ → cavity 1 → PBS₂ → HWP₁). Here

$$\begin{aligned} |\Pi_0\rangle &= |\Pi\rangle^p \otimes |\Pi\rangle_{\text{in}}^e, \\ |\Pi_1\rangle &= |L\rangle_5 |\uparrow\rangle_c |\uparrow\rangle_{t_1} (\alpha_1 |\uparrow\rangle_{t_2} + \alpha_2 |\downarrow\rangle_{t_2}) + |L\rangle_5 |\uparrow\rangle_c |\downarrow\rangle_{t_1} (\alpha_3 |\uparrow\rangle_{t_2} + \alpha_4 |\downarrow\rangle_{t_2}) \\ &\quad + |R\rangle_5 |\downarrow\rangle_c |\uparrow\rangle_{t_1} (\alpha_5 |\uparrow\rangle_{t_2} + \alpha_6 |\downarrow\rangle_{t_2}) + |R\rangle_5 |\downarrow\rangle_c |\downarrow\rangle_{t_1} (\alpha_7 |\uparrow\rangle_{t_2} + \alpha_8 |\downarrow\rangle_{t_2}). \end{aligned} \quad (18)$$

Second, PBS₃ transforms $|R\rangle_5$ and $|L\rangle_5$ into $|R\rangle_6$ and $|L\rangle_7$, respectively. When the photon is in the state $|L\rangle_7$, before and after it goes through the block composed of PBS₅, the QDs inside the cavities 2 and 3, and PBS₇, an H_p is performed on it with HWP₃ and HWP₅, respectively, and then it arrives at the balanced BS directly. When the photon is in the state $|R\rangle_6$, after an H_p is performed on it with HWP₂, the optical switch S leads it to the block composed of PBS₄, the QDs inside the cavities 2 and 3, and PBS₆, following with an H_p which is performed on the photon with a wave plate (WP) and a mirror. Here $|R\rangle_{20} \xrightarrow{\text{WP}} \xrightarrow{\text{mirror}} \xrightarrow{\text{WP}} (|R\rangle_{20} + |L\rangle_{20})/\sqrt{2}$ and $|L\rangle_{20} \xrightarrow{\text{WP}} \xrightarrow{\text{mirror}} \xrightarrow{\text{WP}} (|R\rangle_{20} - |L\rangle_{20})/\sqrt{2}$. These operations (HWP₃ → PBS₅ → cavity 2 → cavity 3 → PBS₇ → HWP₅ and HWP₂ → S → PBS₄ → cavity 2 → cavity 3 → PBS₆ → WP → mirror → WP) complete the transformation

$$\begin{aligned} \rightarrow |\Xi_2\rangle &= |\uparrow\rangle_c |\uparrow\rangle_{t_1} (\alpha_1 |L\rangle_{22} |\uparrow\rangle_{t_2} + \alpha_2 |R\rangle_{22} |\downarrow\rangle_{t_2}) + |\uparrow\rangle_c |\downarrow\rangle_{t_1} (\alpha_1 |R\rangle_{22} |\uparrow\rangle_{t_2} + \alpha_2 |L\rangle_{22} |\downarrow\rangle_{t_2}) \\ &\quad + |\downarrow\rangle_c |\uparrow\rangle_{t_1} (\alpha_1 |R\rangle_{20} |\uparrow\rangle_{t_2} + \alpha_2 |L\rangle_{20} |\downarrow\rangle_{t_2}) + |\downarrow\rangle_c |\downarrow\rangle_{t_1} (\alpha_1 |L\rangle_{20} |\uparrow\rangle_{t_2} + \alpha_2 |R\rangle_{20} |\downarrow\rangle_{t_2}). \end{aligned} \quad (19)$$

Third, the photon emitting from the spatial model 20 is injected into the block composed of PBS₆, the QDs inside the cavities 2 and 3, and PBS₄ again, and before and after the photon interacts with the QDs inside the cavities 3 and 2, an H_e is performed on the QDs inside the cavities 3 and 2, respectively. The optical switch S leads the wave packet to the spatial model 21 for interfering with the wave packet emitting from the spatial model 22. The above operations ($H_{e_2}, H_{e_3} \rightarrow$ PBS₆ → cavity 3 → cavity 2 → PBS₄ → $H_{e_2}, H_{e_3} \rightarrow S$) complete the transformation

$$\begin{aligned} \rightarrow |\Xi_3\rangle &= |\uparrow\rangle_c |\uparrow\rangle_{t_1} (\alpha_1 |L\rangle_{22} |\uparrow\rangle_{t_2} + \alpha_2 |R\rangle_{22} |\downarrow\rangle_{t_2}) + |\uparrow\rangle_c |\downarrow\rangle_{t_1} (\alpha_3 |R\rangle_{22} |\uparrow\rangle_{t_2} + \alpha_4 |L\rangle_{22} |\downarrow\rangle_{t_2}) \\ &\quad + |\downarrow\rangle_c (\alpha_5 |R\rangle_{21} |\uparrow\rangle_{t_1} + \alpha_6 |L\rangle_{21} |\downarrow\rangle_{t_1}) |\uparrow\rangle_{t_2} + |\downarrow\rangle_c (\alpha_7 |L\rangle_{21} |\uparrow\rangle_{t_1} + \alpha_8 |R\rangle_{21} |\downarrow\rangle_{t_1}) |\downarrow\rangle_{t_2}. \end{aligned} \quad (20)$$

Fourth, the single photon is detected by the detectors D_i^\pm in the basis $\{|\pm\rangle\}$ after the 50:50 BS transforms $|\Xi_3\rangle$

into $|\Xi_4\rangle$. Here

$$\begin{aligned}
|\Xi_4\rangle &= \frac{|+\rangle_{25}}{2} \left[|\uparrow\rangle_c |\uparrow\rangle_{t_1} (\alpha_1 |\uparrow\rangle_{t_2} + \alpha_2 |\downarrow\rangle_{t_2}) + |\uparrow\rangle_c |\downarrow\rangle_{t_1} (\alpha_3 |\uparrow\rangle_{t_2} + \alpha_4 |\downarrow\rangle_{t_2}) \right. \\
&\quad \left. + |\downarrow\rangle_c (\alpha_5 |\uparrow\rangle_{t_1} + \alpha_6 |\downarrow\rangle_{t_1}) |\uparrow\rangle_{t_2} + |\downarrow\rangle_c (\alpha_7 |\uparrow\rangle_{t_1} + \alpha_8 |\downarrow\rangle_{t_1}) |\downarrow\rangle_{t_2} \right] \\
&+ \frac{|-\rangle_{26}}{2} \left[|\uparrow\rangle_c |\uparrow\rangle_{t_1} (-\alpha_1 |\uparrow\rangle_{t_2} + \alpha_2 |\downarrow\rangle_{t_2}) + |\uparrow\rangle_c |\downarrow\rangle_{t_1} (\alpha_3 |\uparrow\rangle_{t_2} - \alpha_4 |\downarrow\rangle_{t_2}) \right. \\
&\quad \left. + |\downarrow\rangle_c (\alpha_5 |\uparrow\rangle_{t_1} - \alpha_6 |\downarrow\rangle_{t_1}) |\uparrow\rangle_{t_2} + |\downarrow\rangle_c (-\alpha_7 |\uparrow\rangle_{t_1} + \alpha_8 |\downarrow\rangle_{t_1}) |\downarrow\rangle_{t_2} \right] \\
&+ \frac{|+\rangle_{27}}{2} \left[|\uparrow\rangle_c |\uparrow\rangle_{t_1} (\alpha_1 |\uparrow\rangle_{t_2} + \alpha_2 |\downarrow\rangle_{t_2}) + |\uparrow\rangle_c |\downarrow\rangle_{t_1} (\alpha_3 |\uparrow\rangle_{t_2} + \alpha_4 |\downarrow\rangle_{t_2}) \right. \\
&\quad \left. - |\downarrow\rangle_c (\alpha_5 |\uparrow\rangle_{t_1} + \alpha_6 |\downarrow\rangle_{t_1}) |\uparrow\rangle_{t_2} - |\downarrow\rangle_c (\alpha_7 |\uparrow\rangle_{t_1} + \alpha_8 |\downarrow\rangle_{t_1}) |\downarrow\rangle_{t_2} \right] \\
&+ \frac{|-\rangle_{28}}{2} \left[|\uparrow\rangle_c |\uparrow\rangle_{t_1} (-\alpha_1 |\uparrow\rangle_{t_2} + \alpha_2 |\downarrow\rangle_{t_2}) + |\uparrow\rangle_c |\downarrow\rangle_{t_1} (\alpha_3 |\uparrow\rangle_{t_2} - \alpha_4 |\downarrow\rangle_{t_2}) \right. \\
&\quad \left. + |\downarrow\rangle_c (-\alpha_5 |\uparrow\rangle_{t_1} + \alpha_6 |\downarrow\rangle_{t_1}) |\uparrow\rangle_{t_2} + |\downarrow\rangle_c (\alpha_7 |\uparrow\rangle_{t_1} - \alpha_8 |\downarrow\rangle_{t_1}) |\downarrow\rangle_{t_2} \right]. \tag{21}
\end{aligned}$$

Fifth, according to the outcomes of the measurement on the output single photon, we perform some appropriate classical feed-forward single-qubit operations, shown in Table II, on the electron-spin qubits to make the state of the system composed of the three electrons inside the cavities 1, 2, and 3 to be

$$\begin{aligned}
|\Pi\rangle_{\text{out}}^e &= |\uparrow\rangle_c (\alpha_1 |\uparrow\rangle_{t_1} |\uparrow\rangle_{t_2} + \alpha_2 |\uparrow\rangle_{t_1} |\downarrow\rangle_{t_2}) + |\uparrow\rangle_c (\alpha_3 |\downarrow\rangle_{t_1} |\uparrow\rangle_{t_2} + \alpha_4 |\downarrow\rangle_{t_1} |\downarrow\rangle_{t_2}) \\
&\quad + |\downarrow\rangle_c (\alpha_5 |\uparrow\rangle_{t_1} |\uparrow\rangle_{t_2} + \alpha_6 |\downarrow\rangle_{t_1} |\uparrow\rangle_{t_2}) + |\downarrow\rangle_c (\alpha_7 |\uparrow\rangle_{t_1} |\downarrow\rangle_{t_2} + \alpha_8 |\downarrow\rangle_{t_1} |\downarrow\rangle_{t_2}). \tag{22}
\end{aligned}$$

From Eqs. (18) and (22), one can see that the evolution $|\Pi\rangle_{\text{in}} \xrightarrow{\text{Fredkin}} |\Pi\rangle_{\text{out}}$ is completed. That is, the quantum circuit shown in Fig. 4 implements a Fredkin gate on the three-qubit electron-spin system in a deterministic way, which swaps the states of the two target qubits iff the state of the control qubit is in the state $|\downarrow\rangle$.

TABLE II: The relations between the measurement outcomes of the photon and the feed-forward operations for achieving a Fredkin gate on the three-qubit electron-spin system.

photon	Feed-forward		
	qubit c	qubit t_1	qubit t_2
$D_1^+ (+\rangle_{25})$	I_2	I_2	I_2
$D_1^- (-\rangle_{26})$	$-\sigma_z$	σ_z	σ_z
$D_2^+ (+\rangle_{27})$	σ_z	I_2	I_2
$D_2^- (-\rangle_{28})$	I_2	σ_z	σ_z

V. THE FEASIBILITIES AND EFFICIENCIES OF OUR SCHEMES

So far, all the procedures in our schemes for the three universal quantum gates are described in the case that the side leakage rate k_s is negligible. To present our ideas more realistically, k_s should be taken into account. In this time, the rules of the input states changing under the interaction of the photon and the cavity become

$$\begin{aligned}
|R\rangle |\uparrow\rangle &\xrightarrow{\text{cav}} -|r_0\rangle |R\rangle |\uparrow\rangle, & |L\rangle |\uparrow\rangle &\xrightarrow{\text{cav}} |r_h\rangle |L\rangle |\uparrow\rangle, \\
|R\rangle |\downarrow\rangle &\xrightarrow{\text{cav}} |r_h\rangle |R\rangle |\downarrow\rangle, & |L\rangle |\downarrow\rangle &\xrightarrow{\text{cav}} -|r_0\rangle |L\rangle |\downarrow\rangle. \tag{23}
\end{aligned}$$

The fidelities and the efficiencies of the universal quantum gates are sensitive to k_s as k_s influences the amplitudes of the reflected photon (see Eq. (1)). Here the fidelity of a quantum gate is defined as

$$F = |\langle \Psi_{\text{real}} | \Psi_{\text{ideal}} \rangle|^2, \tag{24}$$

where $|\Psi_{\text{ideal}}\rangle$ is the output state of the system composed of the QD-spin qubits involved in the gate and a single-photon medium in the ideal case (that is, the photon escapes through the input-output mode). $|\Psi_{\text{real}}\rangle$ is the output

state of the complicated system in the realistic case (that is, the cavities are imperfect and the side leakage κ_s is taken into account). The efficiency of the gate is considered as

$$\eta = n_{\text{out}}/n_{\text{in}}. \quad (25)$$

Here n_{in} and n_{out} are the numbers of the input photons and the output photons, respectively.

For perfect cavities, the fidelities of our universal quantum gates can reach unity. By considering the side leakage and combining the specific processes of the construction for the universal quantum gates discussed above, the fidelities of our CNOT gate F_C , Toffoli gate F_T , and Fredkin gate F_F , and their efficiencies η_C , η_T , and η_F can be calculated as follows:

$$F_C = \frac{1}{2} \times (1 + 2|r_h| + |r_0||r_h|) / [(1 + |r_h|)^2 + (1 - |r_0|)^2 + |r_h|^2(1 - |r_h|)^2 + |r_h|^2(1 + |r_0|)^2], \quad (26)$$

$$\begin{aligned} F_T &= \frac{1}{4} \times (3 + 2|r_0| + |r_h|[5 + |r_h| + |r_0|(4 + |r_0|)]) / ((1 + |r_h|)^4 \\ &\quad + 2(|r_h|^2 - 1)^2 + 2(|r_h| - 1)^2(|r_0| - 1)^2 + (|r_0| - 1)^4 + 2(|r_0|^2 - 1)^2 \\ &\quad + 4(1 + |r_h|)^2(1 + |r_0|^2) + |r_h|^2[(|r_h| - 1)^2 + (1 + |r_0|)^2]^2), \end{aligned} \quad (27)$$

$$\begin{aligned} F_F &= \frac{1}{8} \times [4(1 + |r_h|)(1 + |r_0||r_h|) + 2(2 + |r_0| + |r_h|)(2 + |r_0|^2 + |r_h|^2) \\ &\quad + (1 + |r_0|)(4|r_h|^2 - |r_h|^4 + 2|r_h|^3|r_0| + 2|r_h||r_0|^3 + |r_0|^4)] / [(|r_h| - 1)^2 \\ &\quad + (1 + |r_0|)^2][4 + 2(|r_h| - |r_0|)^2 + (|r_h|^2 + |r_0|^2)^2] + 4[(1 + |r_h|)^2 \\ &\quad + (|r_0| - 1)^2][8 + 2(|r_h|^2 + |r_0|^2)^2] + [2 + |r_h|(|r_h| - 2) + |r_0|(2 + |r_0|)] \\ &\quad \times [|r_h|^8 - 4|r_h|^7|r_0| + 4|r_h|^3|r_0|^5 + 8|r_h|^2|r_0|^6 + 4|r_h||r_0|^7 + |r_0|^8 \\ &\quad - 4|r_h|^5|r_0|(|r_0|^2 - 4) + 8|r_h|^6(|r_0|^2 - 1) - 2|r_h|^4(4|r_0|^2 + |r_0|^4 - 8)], \end{aligned} \quad (28)$$

$$\eta_C = \frac{(2 + |r_h|^2 + |r_0|^2)^2}{16}, \quad (29)$$

$$\eta_T = \frac{(2 + |r_h|^2 + |r_0|^2)^2(6 + |r_h|^2 + |r_0|^2)}{128}, \quad (30)$$

$$\eta_F = \frac{(2 + |r_h|^2 + |r_0|^2)[4 + (|r_h|^2 + |r_0|^2)^2][12 + (|r_h|^2 + |r_0|^2)^2]}{512}. \quad (31)$$

It is still a big challenge to achieve strong coupling in experiment at present [15]. However, strong coupling has been observed in the QD-cavity systems with the micropillar form [33, 45–47] and the microdisk form [48, 49], and the QD-nanocavity systems [50] in experiment. In 2004, Reithmaier *et al.* [45] observed $g/(\kappa + \kappa_s) \simeq 0.5$ [$g/(\kappa + \kappa_s) \simeq 2.4$] in a $d = 1.5 \mu\text{m}$ micropillar cavity with a quality factor of $Q = 8800$ [$Q = 40000$]. In 2011, Hu *et al.* [31] demonstrated $g/(\kappa + \kappa_s) \simeq 1.0$ in a micropillar cavity with $\kappa_s/\kappa \simeq 0.7$ and $Q \simeq 1.7 \times 10^4$. In 2010, Loo *et al.* [47] reported $g = 16 \mu\text{eV}$ and $\kappa = 20.5 \mu\text{eV}$ in a $d = 7.3 \mu\text{m}$ micropillar with $Q = 65000$.

The fidelities and the efficiencies of our universal quantum gates, which vary with the coupling strength and the side leakage rate, are shown in Figs. 5 and 6, respectively. From these figures, one can see that our schemes are feasible in both the strong coupling regime and the weak coupling regime. κ_s can be made rather small by improving the sample growth or the etching process.

A QD system has the discrete atom-like energy levels and a spectrum of the ultra-narrow transition that is tunable with the size of the quantum dot. The growth techniques of QDs produce the size variations of the QDs. The spectral line-width inhomogeneous broadening is caused by the fluctuations in the size and shape of a QD, and it has gained the widespread attention [51]. The spectral inhomogeneity is an important property and it is not necessarily a negative consequence for their applications in quantum information processing. The imperfect QD in a realistic system, i.e., the shape of the sample and the strain field distribution are not symmetric, reduces the fidelities of the gates and it can be decreased by designing the shape and the size of the sample or encoding the qubits on a different type of QDs [13, 31].

The information between the photon medium and the QD spins is transferred by the exciton. That is, the exciton dephasing reduces the fidelities of the gates. The exciton dephasing, including the optical dephasing and the spin

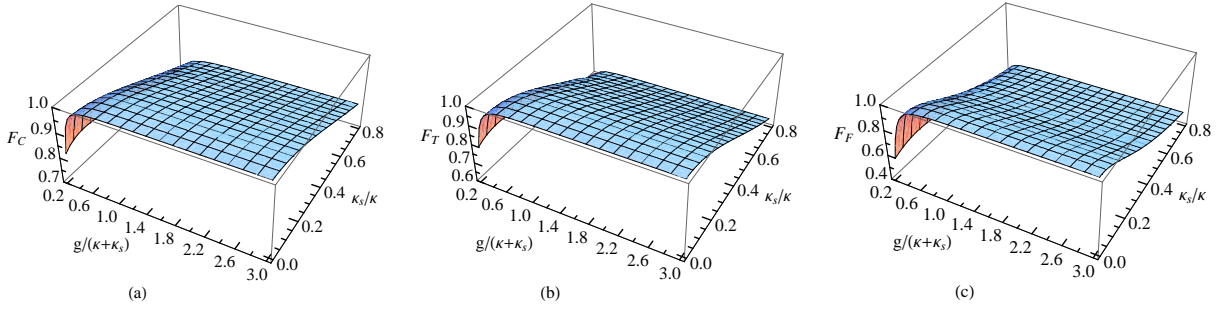


FIG. 5: The fidelities of our universal quantum gates vs the coupling strength $g/(\kappa + \kappa_s)$ and the side leakage rate κ_s/κ . (a) The fidelity of our CNOT gate (F_C). (b) The fidelity of our Toffoli gate (F_T). (c) The fidelity of our Fredkin gate (F_F). We take $\omega = \omega_c = \omega_{X^-}$ and $\gamma/\kappa = 0.1$.

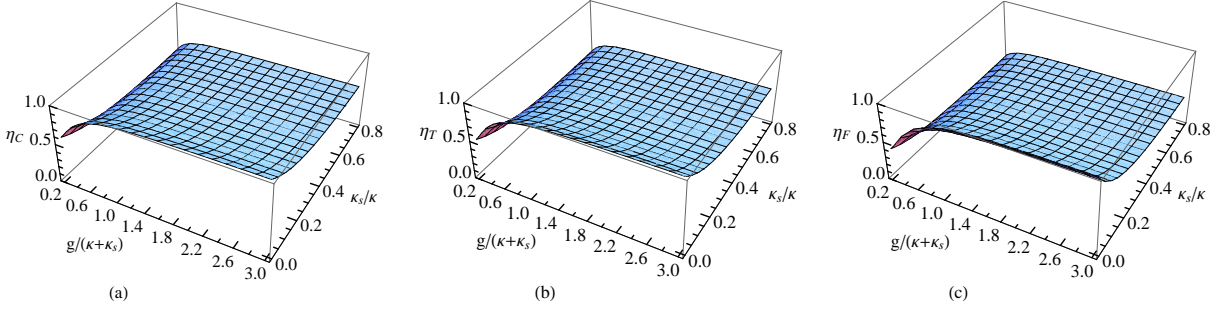


FIG. 6: The efficiencies of our universal quantum gates vs the coupling strength $g/(\kappa + \kappa_s)$ and the side leakage rate κ_s/κ . (a) The efficiency of our CNOT gate (η_C). (b) The efficiency of our Toffoli gate (η_T). (c) The efficiency of our Fredkin gate (η_F). We take $\omega = \omega_c = \omega_{X^-}$ and $\gamma/\kappa = 0.1$.

dephasing, is sensitive to the dipole coherence time T_2 and the cavity-photon coherence time τ . The exciton dephasing reduces the fidelities of the universal quantum gates less than 10% as it reduces the fidelities by a factor

$$1 - \exp(-\tau/T_2), \quad (32)$$

and the ultralong optical coherence time of the dipole T_2 can reach several picoseconds at a low temperature [52, 53], while the cavity-photon coherence time τ is around 10 picoseconds in a InGaAs QD. The QD-hole spin coherence time T_2 is long more than 100 nanoseconds [54].

VI. DISCUSSION AND SUMMARY

Quantum logic gates are essential building blocks in quantum computing and quantum information processing [1]. CNOT gates are used widely in quantum computing. Directly physical realization of multiqubit gates is a main direction as the optimal length of the unconstructed circuit for a generic n -qubit gate is $[(4^n - 3n - 1)/4]$ [55].

Some significant progress has been made in realizing universal quantum gates. Refs. [14, 15, 23] present some interesting schemes for the quantum gates on hybrid light-matter or electron-nuclear qubits. Based on parity-check gates, the CNOT gate on moving electron qubits is proposed in 2004, assisted by an additional electron qubit [11]. A Toffoli gate on atom qubits with a success probability of 1/2 is constructed by Wei *et al.* in 2008 [56]. Our CNOT, Toffoli, and Fredkin gates are compact, simple, and economic as the ancilla qubits, employed in [9–11], are not required, and only a single-photon medium is employed. The proposals for the Toffoli and Fredkin gates beat their synthesis with two-qubit entangling gates and single-qubit gates largely. The optimal synthesis of a three-qubit Toffoli gate requires six CNOT gates [57] and five quantum entangling gates on two individual qubits are required to synthesize a three-qubit Fredkin gate [58]. All our schemes are deterministic and the qubits for the gates are stationary. The side leakage rate of a single-side cavity is usually lower than that of a double-side one [41]. Moreover, a QD is easier to be confined in a cavity than an atom [34, 59].

In summary, we have proposed some compact schemes for implementing quantum computing on solid-state electron-spin qubits in the QDs assisted by single-side resonant optical microcavities in a deterministic way. Based on the fact

that the R -polarized and the L -polarized photons reflected by the QD-cavity contribute different phase shifts, the compact quantum circuits for the CNOT, Toffoli, and Fredkin gates on the stationary electron-spin qubits are achieved by some input-output processes of a single-photon medium and some classical feed-forward operations. Our proposals are compact and economic as the additional QD-spin qubits are not required and our schemes for implementing the multiqubit gates beat their synthesis with two-qubit entangling gates and single-qubit gates largely. The success probabilities of our universal quantum gates are 100% in principle. With current technology, our schemes are feasible. Together with single-qubit gates, our universal quantum gates are sufficient for any quantum computing in solid-state QD-spin systems.

Acknowledgments

This work is supported by the National Natural Science Foundation of China under Grant No. 11174039, NECT-11-0031, and the Open Foundation of State key Laboratory of Networking and Switching Technology (Beijing University of Posts and Telecommunications) under Grant No. SKLNST-2013-1-13.

-
- [1] M. A. Nielsen and I. L. Chuang, *Quantum Computation and Quantum Information* (Cambridge University, Cambridge, 2000).
 - [2] A. Barenco, C. H. Bennett, R. Cleve, D. P. DiVincenzo, N. Margolus, P. Shor, T. Sleator, J. A. Smolin, and H. Weinfurter, "Elementary gates for quantum computation," *Phys. Rev. A* **52**, 3457-3457 (1995).
 - [3] Y. Y. Shi, "Both Toffoli and controlled-not need little help to do universal quantum computation," *Quantum Inf. Comput.* **3**, 084-092 (2003).
 - [4] E. Fredkin and T. Toffoli, "Conservative logic," *Int. J. Theor. Phys.* **21**, 219-253 (1982).
 - [5] G. L. Long and L. Xiao, "Parallel quantum computing in a single ensemble quantum computer," *Phys. Rev. A* **69**, 052303 (2004).
 - [6] G. F. Xu, J. Zhang, D. M. Tong, E. Sjöqvist, and L. C. Kwek, "Nonadiabatic holonomic quantum computation in decoherence-free subspaces," *Phys. Rev. Lett.* **109**, 170501 (2012).
 - [7] G. R. Feng, G. F. Xu, and G. L. Long, "Experimental realization of nonadiabatic holonomic quantum computation," *Phys. Rev. Lett.* **110**, 190501 (2013).
 - [8] E. Knill, R. Laflamme, and G. J. Milburn, "A scheme for efficient quantum computation with linear optics," *Nature (London)* **409**, 46-52 (2001).
 - [9] K. Nemoto and W. J. Munro, "Nearly deterministic linear optical controlled-not gate," *Phys. Rev. Lett.* **93**, 250502 (2004).
 - [10] Q. Lin and J. Li, "Quantum control gates with weak cross-Kerr nonlinearity," *Phys. Rev. A* **79**, 022301 (2009).
 - [11] C. W. J. Beenakker, D. P. DiVincenzo, C. Emary, and M. Kindermann, "Charge detection enables free-electron quantum computation," *Phys. Rev. Lett.* **93**, 020501 (2004).
 - [12] C. Y. Hu, A. Young, J. L. O'Brien, W. J. Munro, and J. G. Rarity, "Giant optical Faraday rotation induced by a single-electron spin in a quantum dot: Applications to entangling remote spins via a single photon," *Phys. Rev. B* **78**, 085307 (2008).
 - [13] C. Y. Hu, W. J. Munro, and J. Rarity, "Deterministic photon entangler using a charged quantum dot inside a microcavity," *Phys. Rev. B* **78**, 125318 (2008).
 - [14] C. Bonato, F. Haupt, S. S. R. Oemrawsingh, J. Gudat, D. Ding, M. P. van Exter, and D. Bouwmeester, "CNOT and Bell-state analysis in the weak-coupling cavity QED regime," *Phys. Rev. Lett.* **104**, 160503 (2010).
 - [15] H. R. Wei and F. G. Deng, "Universal quantum gates for hybrid systems assisted by quantum dots inside doubled-sided optical microcavities," *Phys. Rev. A* **87**, 022305 (2013).
 - [16] H. R. Wei and F. G. Deng, "Scalable photonic quantum computing assisted by quantum-dot spin in double-sided optical microcavity," *Opt. Express* **21**, 17671-17685 (2013).
 - [17] H. F. Wang, A. D. Zhu, S. Zhang, and K. H. Yeon, "Optically controlled phase gate and teleportation of a controlled-NOT gate for spin qubits in a quantum-dot-microcavity coupled system," *Phys. Rev. A* **87**, 062337 (2013).
 - [18] X. Li, Y. Wu, D. Steel, D. Gammon, T. H. Stievater, and D. S. Katzer, "An all-optical quantum gate in a semiconductor quantum dot," *Science* **301**, 809-811 (2003).
 - [19] B. C. Ren, H. R. Wei, and F. G. Deng, "Deterministic photonic spatial-polarization hyper-controlled-not gate assisted by quantum dot inside one-side optical microcavity," *Laser Phys. Lett.* **10**, 095202 (2013).
 - [20] T. Yamamoto, Y. A. Pashkin, O. Astafiev, Y. Nakamura, and J. S. Tsai, "Demonstration of conditional gate operation using superconducting charge qubits," *Nature (London)* **425**, 941-944 (2003).
 - [21] J. Clarke and F. K. Wilhelm, "Superconducting quantum bits," *Nature (London)* **453**, 1031-1042 (2008).
 - [22] W. L. Yang, Z. Q. Yin, Z. Y. Xu, M. Feng, and J. F. Du, "One-step implementation of multiqubit conditional phase gating with nitrogen-vacancy centers coupled to a high-Q silica microsphere cavity," *Appl. Phys. Lett.* **96**, 241113 (2010).
 - [23] F. Jelezko, T. Gaebel, I. Popa, M. Domhan, A. Gruber, and J. Wrachtrup, "Observation of coherent oscillation of a single nuclear spin and realization of a two-qubit conditional quantum gate," *Phys. Rev. Lett.* **93**, 130501 (2004).

- [24] B. C. Ren and F. G. Deng, "Hyperentanglement purification and concentration assisted by diamond NV centers inside photonic crystal cavities," *Laser Phys. Lett.* **10**, 115201 (2013).
- [25] J. R. Petta, A. C. Johnson, J. M. Taylor, E. A. Laird, A. Yacoby, M. D. Lukin, C. M. Marcus, M. P. Hanson, and A. C. Gossard, "Coherent manipulation of coupled electron spins in semiconductor quantum dots," *Science* **309**, 2180-2184 (2005).
- [26] A. Greilich, D. R. Yakovlev, A. Shabaev, A. L. Efros, I. A. Yugova, R. Oulton, V. Stavarache, D. Reuter, A. Wieck, and M. Bayer, "Mode locking of electron spin coherences in singly charged quantum dots," *Science* **313**, 341-345 (2006).
- [27] D. Press, K. De Greve, P. L. McMahon, T. D. Ladd, B. Friess, C. Schneider, M. Kamp, S. Höfling, A. Forchel, and Y. Yamamoto, "Ultrafast optical spin echo in a single quantum dot," *Nature Photon.* **4**, 367-370 (2010).
- [28] J. Berezovsky, M. H. Mikkelsen, N. G. Stoltz, L. A. Coldren, and D. D. Awschalom, "Picosecond coherent optical manipulation of a single electron spin in a quantum dot," *Science* **320**, 349-352 (2008).
- [29] D. Press, T. D. Ladd, B. Y. Zhang, and Y. Yamamoto, "Complete quantum control of a single quantum dot spin using ultrafast optical pulses," *Nature (London)* **456**, 218-221 (2008).
- [30] J. A. Gupta, R. Knobel, N. Samarth, and D. D. Awschalom, "Ultrafast manipulation of electron spin coherence," *Science* **292**, 2458-2461 (2001).
- [31] C. Y. Hu and J. G. Rarity, "Loss-resistant state teleportation and entanglement swapping using a quantum-dot spin in an optical microcavity," *Phys. Rev. B* **83**, 115303 (2011).
- [32] D. F. Walls and G. J. Milburn, *Quantum Optics* (Springer-Verlag, Berlin, 1994).
- [33] A. B. Young, R. Oulton, C. Y. Hu, A. C. T. Thijssen, C. Schneider, S. Reitzenstein, M. Kamp, and S. Höfling, "Quantum-dot-induced phase shift in a pillar microcavity," *Phys. Rev. A* **84**, 011803 (2011).
- [34] L. M. Duan and H. J. Kimble, "Scalable photonic quantum computation through cavity-assisted interactions," *Phys. Rev. Lett.* **92**, 127902 (2004).
- [35] C. Bonato, D. Ding, J. Gudat, S. Thon, H. Kim, P. M. Petroff, M. P. van Exter, and D. Bouwmeester, "Tuning micropillar cavity birefringence by laser induced surface defects," *Appl. Phys. Lett.* **95**, 251104 (2009).
- [36] J. Gudat, C. Bonato, E. van Nieuwenburg, S. Thon, H. Kim, P. M. Petroff, M. P. van Exter, and D. Bouwmeester, "Permanent tuning of quantum dot transitions to degenerate microcavity resonances," *Appl. Phys. Lett.* **98**, 121111 (2011).
- [37] C. Bonato, E. van Nieuwenburg, J. Gudat, S. Thon, H. Kim, M. P. van Exter, and D. Bouwmeester, "Strain tuning of quantum dot optical transitions via laser-induced surface defects," *Phys. Rev. B* **84**, 075306 (2011).
- [38] I. J. Luxmoore, E. D. Ahmadi, B. J. Luxmoore, N. A. Wasley, A. I. Tartakovskii, M. Hugues, M. S. Skolnick, and A. M. Fox, "Restoring mode degeneracy in H1 photonic crystal cavities by uniaxial strain tuning," *Appl. Phys. Lett.* **100**, 121116 (2012).
- [39] J. Hagemeyer, C. Bonato, T. A. Truong, H. Kim, G. J. Beirne, M. Bakker, M. P. van Exter, Y. Q. Luo, P. Petroff, and D. Bouwmeester, "H1 photonic crystal cavities for hybrid quantum information protocols," *Opt. Express* **20**, 24714 (2012).
- [40] R. Albrecht, A. Bommer, C. Deutsch, J. Reichel, and C. Becher, "Coupling of a single nitrogen-vacancy center in diamond to a fiber-based microcavity," *Phys. Rev. Lett.* **110**, 243602 (2013).
- [41] C. Y. Hu, W. J. Munro, J. L. O'Brien, and J. G. Rarity, "Proposed entanglement beam splitter using a quantum-dot spin in a double-sided optical microcavity," *Phys. Rev. B* **80**, 205326 (2009).
- [42] A. B. Young, C. Y. Hu, and J. G. Rarity, "Generating entanglement with low-Q-factor microcavities," *Phys. Rev. A* **87**, 012332 (2013).
- [43] B. C. Ren, H. R. Wei, M. Hua, T. Li, and F. G. Deng, "Complete hyperentangled-bell-state analysis for photon systems assisted by quantum-dot spins in optical microcavities," *Opt. Express* **20**, 24664-24677 (2012).
- [44] T. J. Wang, S. Y. Song, and G. L. Long, "Quantum repeater based on spatial entanglement of photons and quantum-dot spins in optical microcavities," *Phys. Rev. A* **85**, 062311 (2012).
- [45] J. P. Reithmaier, G. Sek, A. Löffler, C. Hofmann, S. Kuhn, S. Reitzenstein, L. V. Keldysh, V. D. Kulakovskii, T. L. Reinecke, and A. Forchel, "Strong coupling in a single quantum dot-semiconductor microcavity system," *Nature (London)* **432**, 197-200 (2004).
- [46] S. Reitzenstein, C. Hofmann, A. Gorbunov, M. Strauß, S. H. Kwon, C. Schneider, A. Löffler, S. Höfling, M. Kamp, and A. Forchel, "AlAs/GaAs micropillar cavities with quality factors exceeding 150,000," *Appl. Phys. Lett.* **90**, 251109 (2007).
- [47] V. Loo, L. Lanco, A. Lemaître, I. Sagnes, O. Krebs, P. Voisin, and P. Senellart, "Quantum dot-cavity strong-coupling regime measured through coherent reflection spectroscopy in a very high-Q micropillar," *Appl. Phys. Lett.* **97**, 241110 (2010).
- [48] E. Peter, P. Senellart, D. Martrou, A. Lemaître, J. Hours, J. M. Gérard, and J. Bloch, "Exciton-photon strong-coupling regime for a single quantum dot embedded in a microcavity," *Phys. Rev. Lett.* **95**, 067401 (2005).
- [49] C. P. Michael, K. Srinivasan, T. J. Johnson, O. Painter, K. H. Lee, K. Hennessy, H. Kim, and E. Hu, "Wavelength- and material-dependent absorption in GaAs and AlGaAs microcavities," *Appl. Phys. Lett.* **90**, 051108 (2007).
- [50] T. Yoshie, A. Scherer, J. Hendrickson, G. Khitrova, H. M. Gibbs, G. Rupper, C. Ell, O. B. Shchekin, and D. G. Deppe, "Vacuum Rabi splitting with a single quantum dot in a photonic crystal nanocavity," *Nature (London)* **432**, 200-203 (2004).
- [51] J. Cui, A. P. Beyler, L. F. Marshall, O. Chen, D. K. Harris, D. D. Wanger, X. Brokmann, and M. G. Bawendi, "Direct probe of spectral inhomogeneity reveals synthetic tunability of single-nanocrystal spectral linewidths," *Nature Chemistry* **5**, 602 (2013).
- [52] P. Borri, W. Langbein, S. Schneider, U. Woggon, R. L. Sellin, D. Ouyang, and D. Bimberg, "Ultralong dephasing time in

- InGaAs quantum dots,” *Phys. Rev. Lett.* **87**, 157401 (2001).
- [53] D. Birkedal, K. Leosson, and J. M. Hvam, “Long lived coherence in self-assembled quantum dots,” *Phys. Rev. Lett.* **87**, 227401 (2001).
- [54] D. Brunner, B. D. Gerardot, P. A. Dalgarno, G. Wüst, K. Karrai, N. G. Stoltz, P. M. Petroff, and R. J. Warburton, “A coherent single-hole spin in a semiconductor,” *Science* **325**, 70-72 (2009).
- [55] V. V. Shende, I. L. Markov, and S. S. Bullock, “Minimal universal two-qubit controlled-NOT-based circuits,” *Phys. Rev. A* **69**, 062321 (2004).
- [56] H. Wei, W. L. Yang, Z. B. Deng, and M. Feng, “Many-qubit network employing cavity QED in a decoherence-free subspace,” *Phys. Rev. A* **78**, 014304 (2008).
- [57] V. V. Shende and I. L. Markov, “On the CNOT-cost of Toffoli gate,” *Quant. Inf. Comput.* **9**, 0461-0468 (2009).
- [58] J. A. Smolin and D. P. DiVincenzo, “Five two-bit quantum gates are sufficient to implement the quantum Fredkin gate,” *Phys. Rev. A* **53**, 2855-2856 (1996).
- [59] J. H. An, M. Feng, and C. H. Oh, “Quantum-information processing with a single photon by an input-output process with respect to low-Q cavities,” *Phys. Rev. A* **79**, 032303 (2009).